frontiers | Frontiers in Chemistry

TYPE Original Research
PUBLISHED 04 March 2024
DOI 10.3389/fchem.2024.1378332



OPEN ACCESS

EDITED BY
Qingping Ding,
Iowa State University, United States

REVIEWED BY
Weitang Yao,
Chengdu University, China
Shubo Cheng,
Yangtze University, China

*CORRESPONDENCE
Wenfeng Liu,
193902015@csu.edu.cn
Jicheng Zhou,
jicheng@csu.edu.cn

RECEIVED 29 January 2024
ACCEPTED 26 February 2024
PUBLISHED 04 March 2024

CITATION
Liu W, Zhou Z and Zhou J (2024), Optimization of doping design for planar P-N homologous junction perovskite solar cells.
*Front. Chem.* 12:1378332.
doi: 10.3389/fchem.2024.1378332



# Optimization of doping design for planar P-N homologous junction perovskite solar cells

Wenfeng Liu[1]*, Ziyou Zhou[2] and Jicheng Zhou[1]*

[1]School of Energy Science and Engineering, Central South University, Changsha, China, [2]School of Materials Science and Engineering, Central South University, Changsha, China

In this study, we used the solar cell capacitance simulator (SCAPS) to analyse numerically the performance of perovskite solar cells (PSCs) containing $CH_3NH_3PbI_3$. The findings indicate that P-N homologous junction processing based on traditional P-I-N PSCs can enhance the photoelectric conversion efficiency (PCE). Furthermore, the authors analyzed the effect of uniform P-N doping of $CH_3NH_3PbI_3$, concluding that the photoelectric efficiency can be improved from 16.10% to 19.03% after doping. In addition, the optical properties of PSCs under solar irradiation are simulated using finite difference time-domain (FDTD) software under AM1.5. This method is applied to investigate the effect of the P-N uniform junction on the internal electric field generated within the cell. The generation of this electric field promotes carrier separation and transmission, ultimately increasing the open circuit voltage ($V_{OC}$) of the solar cell from 1.03 to 1.12 V. The usage of P-N junctions enhances PSCs performance and exhibits vast potential for designing and developing PSCs.

KEYWORDS

**P-N homogeneous, perovskite solar cells, performance optimization, solar energy absorption, doping design**

## 1 Introduction

In recent years, solar energy has been gaining more attention from researchers because of its great potential in photovoltaic power generation, photothermal reaction and inexhaustible (Zhu Y. Y. et al., 2023; Fu et al., 2024). At present, with the deepening of research and the continuous progress of technology, the cost of solar leveled electricity is constantly reduced, and solar energy and traditional energy have greater competitiveness (Maksimovic et al., 2022; Xiao et al., 2023; Zheng Y. et al., 2024). Traditional silicon based solar cells are relatively mature, but there are many problems such as complex preparation and high cost (Zhang H. et al., 2023). In recent years, perovskite light-absorbing materials have been broadly used in solar cells because of their excellent optical properties, high photoelectric conversion rate, high light absorption coefficient, low price and relatively simple preparation (Kim et al., 2012; Shangguan et al., 2022a; Shen et al., 2022; Liang S. et al., 2023; Seyed-Talebi et al., 2023). Since the first PSCs was fabricated in 2009, the PCE has increased from 3.8% to 26.1% (Akihiro et al., 2009; Park et al., 2023). PSCs are a new photovoltaic technology that utilises a class of materials with a special crystal structure, called perovskite materials, as a light-absorbing layer to convert solar energy into electricity. The advantages of perovskite materials, such as high efficiency, low cost, adjustability and flexibility, have enabled PSCs to surpass the efficiency of crystalline silicon solar cells in the laboratory, making them one of the most promising third-generation photovoltaic technologies. There are two common PSCs device structures: a mesoporous structure based on dye-sensitised solar cells (DSSCs) and a planar structure based

on solid-state hole transport layers (HTLs). Among them, the planar structures can be further classified into P-I-N and N-I-P types, which are named according to the order of their electrodes. In recent years, researchers have largely improved the PCE by reducing carrier recombination loss in perovskite layers and interlayer interfaces (Cui et al., 2019; Sengar et al., 2021; Zhang C. et al., 2022). P-N homologous junction PSCs offer the advantage of avoiding the need for organic hole transport layers (HTLs), which reduces the cost and instability associated with organic materials. Additionally, these junctions can achieve higher $V_{OC}$ due to their built-in electric field, resulting in effective separation of the photogenerated carriers and reduced interfacial recombination and ohmic losses. Therefore, they have the potential to significantly enhance the PCE (Sengar et al., 2021). Faced with this situation, a planar perovskite cell with P-N homogeneous junction with an efficiency up to 21.3% was proposed (Cui et al., 2019). This structure can further reduce carrier recombination to improve the photoelectron collection efficiency. Because there is an internal electric field in P-N homogeneous perovskite, which can amplify the directional transport of electrons and holes, the efficiency of photoelectric conversion can be improved (He et al., 2021). In this regard, Daniyal Khosh Maram et al. designed a homogeneous junction solar cell with a PCE of more than 3% in 2021 (Maram et al., 2021). Zhang Yutao et al. of Nanjing University of Technology used FDTD to design a new PSCs, obtaining a series of optical performance parameters of the model (Zhang and Xuan, 2016).

The perovskite material's properties dictate a high light absorption coefficient, allowing it to absorb all incident photons in the solar cell at just 300 nm thickness. Furthermore, the material boasts a large dielectric constant. The perovskite material analysed in this study has a thickness of 320 nm, and photons absorbed in the photosensitive layer of the perovskite separate the electron-hole pairs, generating free electrons and holes even at room temperature. However, there is a limited issue with the PCE of conventional P-I-N PSCs (Verschraegen and Marc, 2007; You et al., 2016; Chatterji and Pradeep, 2019), and the impact of analogous P-N junction on conventional PSCs is being examined.

In this investigation, the $CH_3NH_3PbI_3$ PSCs were numerically analysed by employing the solar cell capacitance simulator (SCAPS), and the PCE was enhanced following the P-N analogous junction treatment of the conventional outcomes (Peng et al., 2019). The effectiveness of the device model in simulation is verified by comparing with the experiment results. Systematic analysis of P-N homojunction shows that PSCs with P-N homojunction perovskite have better $V_{OC}$ and Filling Factor (FF) than ordinary structures (Mohamad et al., 2023). The application of P-N homogeneous junction has great potential in the design and development of PSCs (Lin et al., 2019).

## 2 Structure design and simulation

We used SCAPS-1D software to perform simulation calculations on PSCs, and the material geometric parameters of the cells were consistent with the experimental reports (You et al., 2016; Chatterji and Pradeep, 2019). The thicknesses of perovskite layer ($CH_3NH_3PbI_3$), hole transport layer (NiO) and electron transport layer (ZnO) were 320 nm, 80 nm and 70 nm respectively (see Figure 1A for detailed models). Next, P-$CH_3NH_3PbI_3$ is as thick as N- by converting the P-I-N of $CH_3NH_3PbI_3$ to the P-N homologous junction structure of P-$CH_3NH_3PbI_3$ (see Figure 1B). Standard AM1.5 G spectrum is used as incident light source for simulation calculation. All material parameters of each layer in simulation are listed in Table 1.

Figure 1 is Original 3D structure diagram of $CH_3NH_3PbI_3$ PSCs and PN homologous cell structure diagram. We can see from this figure that this PSCs is composed of ZnO/n-type perovskite/p-type perovskite/NiO. The specific structural parameters are consistent with those in previous experimental study (Akihiro et al., 2009). Table 1 shows the parameters of each material, including material thickness, energy level and doping thickness (Huang et al., 2016; An et al., 2018; Haider et al., 2018; Vallisree et al., 2018; Azri et al., 2019; Chang et al., 2019). Figure 1B shows the structure diagram after P-N homology, which is based on the $CH_3NH_3PbI_3$ material with PN junction doping. In the table, the specific parameters are as follows: Eg is the band gap of the material, εr is the relative dielectric constant of the material, χ is the electron affinity of the material, μe and μh are the mobility of electrons and holes, NA and ND are the doping concentrations of acceptor and donor, NC and NV are the densities of effective states in the conduction band and valence band.

The Finite Difference in Time Domain (FDTD) method was utilized to examine the characteristics of light waves in Planar P-N homologous junction solar cells. To calculate the electromagnetic light waves and observe the interactions between layers in the PSCs structure, Maxwell's equations were employed. This method was selected due to its broad spectrum of bands, computational potency, and high level of precision (Lu et al., 2023; Li et al., 2024a; He et al., 2024). In this study, we use the complex refractive index of the material in the cell structure as input for optical simulation. However, we are unable to obtain the structure using only the differential equations for electromagnetic field distribution with time and space, and also require the assistance of boundary conditions. Figure 1C depicts the P-N homojunction PSCs positioned in the air for calculation. We utilised a specific grid size of 5 nm and a mesh accuracy of 3 to maximise simulation accuracy. A Perfectly Matched Layer (PML) served as the absorbing boundary at the upper and lower interfaces of the structure, while Periodic Boundary Conditions (PBC) were employed at the left and right interfaces of the structure. By placing a reflection monitor at the top of the structure, it is possible to calculate the reflection coefficient R (Shangguan et al., 2022b; Li W. X. et al., 2023; Ma et al., 2023a; Li et al., 2024b). Similarly, by placing a transmission monitor at the bottom of the structure, the transmission coefficient T can be calculated. This enables the absorptivity of the entire structure to be calculated as A = 1-R-T, giving the absorptivity of the entire solar cell (Zhang Y. X. et al., 2022; Ma et al., 2023b; Lu et al., 2024).

Where T denotes transmittance and R denotes reflectivity, reflectance is defined as the ratio of the intensity of reflected light to incident light. When sunlight strikes the surface of PSCs and contact vertically, its reflection coefficient can be expressed as follows Eq. 1 (Zheng R. Y. et al., 2024; Liu et al., 2024):

$$R = \frac{(n-1)^2 + k^2}{(n+1)^2 + k^2} \quad (1)$$

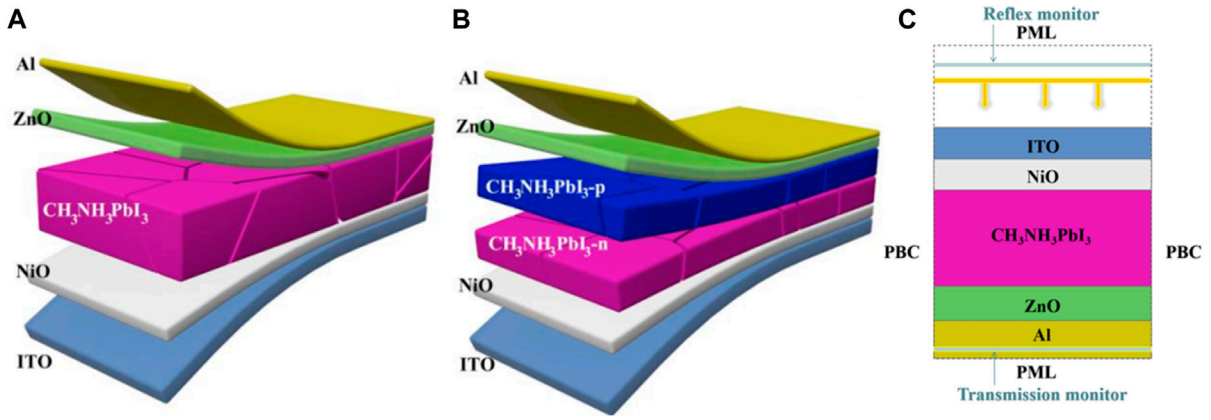


FIGURE 1
**(A)** P-I-N cell structure diagram,**(B)** P-N homologous cell structure diagram, **(C)** FDTD model diagram.

**TABLE 1** Material parameters used for simulation.

| Parameter | ZnO (Vallisree et al., 2018; Azri et al., 2019) | $MAPbI_3$ (Huang et al., 2016; An et al., 2018; Haider et al., 2018) | NiO (Chang et al., 2019) | P-$MAPbI_3$ | N-$MAPbI_3$ |
|---|---|---|---|---|---|
| Thickness (nm) | 70 | 320 | 80 | 160 | 160 |
| Eg (eV) | 3.30 | 1.55 | 3.60 | 1.55 | 1.55 |
| $\varepsilon_r$ | 9.00 | 6.50 | 10.70 | 6.50 | 6.50 |
| $\chi$(eV) | 4.20 | 3.90 | 1.70 | 3.90 | 3.90 |
| $\mu_e/\mu_h$ ($cm^2/Vs$) | 100/25 | 2/2 | 12/2.8 | 2/2 | 2/2 |
| $N_A$ | 0 | — | 2.0E16 | 5.0E18 | 0 |
| $N_D$ | 1.0E18 | — | 0 | 0 | 5.0E14 |
| $N_c$ | 2.2E18 | 2.2E18 | 2.8E19 | 2.2E18 | 2.2E18 |
| $N_v$ | 1.8E19 | 1.8E19 | 1.0E19 | 1.8E19 | 1.8E19 |

Where 'n' represents the ratio of light velocity in a vacuum to light velocity in the semiconductor, and 'k' represents the extinction coefficient. Light scattering is a phenomenon that describes changes in the direction of light transmission after entering a medium. In PSCs, light scattering can enhance the path of light, which increases the cell's exposure to sunlight and thus results in secondary absorption. Finite-difference time-domain (FDTD) software that is based on Maxwell's equations has been extensively employed in the simulation of solar cell (Guo et al., 2022). The Maxwell's equations is expressed as follows Eqs 2, 3 (Li et al., 2023b):

$$\frac{\partial E}{\partial t} = \frac{1}{\varepsilon}\nabla \times H - \frac{1}{\varepsilon}(J + \sigma E) \quad (2)$$

$$\frac{\partial H}{\partial t} = -\frac{1}{\mu}\nabla \times E - \frac{1}{\mu}(M + \sigma_m M) \quad (3)$$

The Lumerical FDTD method, which is used to simulate micro-nanophotonic devices, relies on Maxwell's equations as its foundation (Zhu W. L. et al., 2023). These equations are critical to the analysis of the simulation.

## 3 Result and discussion

Figures 2A, B present line charts depicting the impact of the P-type absorbing layer's doping concentration on FF, PCE, $V_{OC}$, and short-circuit current ($J_{SC}$). The charts provide a quantitative analysis of the aforementioned factors. Figures 2C, D illustrates the impact of the doping concentration in the N-type absorbing layer on the FF, PCE, $V_{OC}$, and $J_{SC}$, presented using line plots. It is evident from Figure 2 that the PCE of solar cells significantly depends on the doping concentration of the P-type and N-type absorbing layers (Wang et al., 2022a). Therefore, optimizing the doping parameters is crucial to achieve the most optimal outcome. Figure 2 illustrates that the doping concentration of both P-type and N-type absorption layers has an impact on the $V_{OC}$ and $J_{SC}$ of the solar cell, as well as its maximum power point position and maximum power value.

After optimal doping concentration, we can find that P-N homojunction can lead to increased energy band bending in the perovskite layer, which increases the $V_{OC}$. The $V_{OC}$ is the output voltage of a solar cell when there is no external load, which reflects the maximum output capacity of the solar cell. Energy band bending

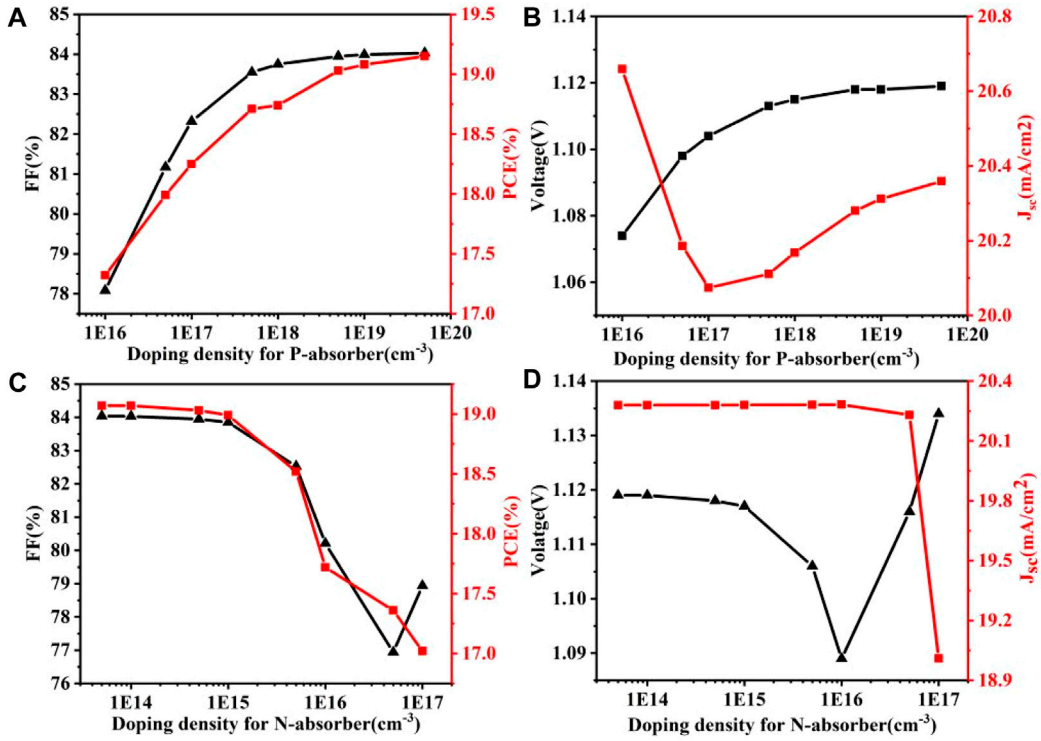


FIGURE 2
Effects of different types of absorbent doping concentrations on FF, PCE, $V_{OC}$ and $J_{SC}$, respectively, **(A,B)** P-type absorber; **(C,D)** N-type absorber.

is the energy difference between the conduction and valence bands in different regions of a semiconductor material, which affects the separation and collection efficiency of carriers. P-N homojunction increases the $V_{OC}$ by forming a larger energy band bending in the perovskite layer (He et al., 2022; Liang S. R. et al., 2023). To further analyse the effect of P-N homojunction on cell performance, we calculated the amount of composite cells and compared it with conventional P-I-N type PSCs as shown in Figure 3A. Composite is a process where photogenerated carriers (i.e., light-excited electrons and holes) recombine inside the device and disappear, and it reduces the efficiency of the solar cell. In Figure 3C, The dotted line shows the simulated P-N interface of P-N homojunction PSCs. We can see that the P-N homojunction PSCs has a lower amount of composite throughout the device compared to the conventional P-I-N PSCs under the same conditions. This indicates that the P-N homojunction can effectively inhibit carrier complexation. However, in Figure 3B, we can also notice that the amount of compounding increases in the P-type region (i.e., undoped region) away from the P-N interface (i.e., doped region). This is due to the fact that the P-N homojunction generates a reverse built-in electric field in this region, which promotes carrier complexation (Wang et al., 2022b).

To verify this, we also calculated the cell carrier density distribution and compared it with a conventional P-I-N PSCs. Carrier density is the number of carriers present per unit volume, which reflects the light absorption and photovoltaic conversion efficiency of the solar cell. As shown in Figure 3D, we can see that in the P-type perovskite region close to the hole transport layer (HTL), the electron density of the P-N homojunction PSCs is significantly lower and the hole density is significantly higher compared to the conventional P-I-N PSCs. This indicates that the P-N homojunction generates a positive built-in electric field in this region, which promotes the directional transport of carriers. Directional transport means that the carriers move in the direction of the built-in electric field, thus increasing the output current of the solar cell.

Figure 4A shows the ITO/NiO/$CH_3NH_3PbI_3$/ZnO/Al structure of solar cell simulation and the experiment of J-V characteristic curve contrast figure. By observing the data results, we can know that the results of simulation and experiment are basically the same, which verifies the validity of the simulation results. The model was transformed into a perovskite P-N homogeneous cell with N-$CH_3NH_3PbI_3$ concentration of 5e14 $cm^{-3}$ and P-$CH_3NH_3PbI_3$ concentration of 5e18 $cm^{-3}$. The PCE of the new cell is 19.03%, which is 18.20% higher than the original one. The $V_{OC}$ is improved from 1.03 V to 1.12 V, and the filling factor (FF) is increased from 75.13% to 83.95%. In the comparison of P-N homologous junction cells and conventional P-I-N cells, the increase of $V_{OC}$ and FF in P-N homologous junction cells is much larger than the decrease of $J_{SC}$ of P-N homologous junction cells, which is also the reason for the improvement of PCE of P-N homologous junction cells as shown in Figures 3A, 4B. In view of the influence of doping concentration on conversion efficiency of P-N homojunction solar cells, P-N junction with different doping concentration was selected according to Figure 2, and the conversion efficiency was calculated and analyzed. It was concluded that the perovskite with N-$CH_3NH_3PbI_3$ concentration of 5e14 $cm^{-3}$ and P-$CH_3NH_3PbI_3$ concentration of 5e18 $cm^{-3}$ has the best conversion efficiency.

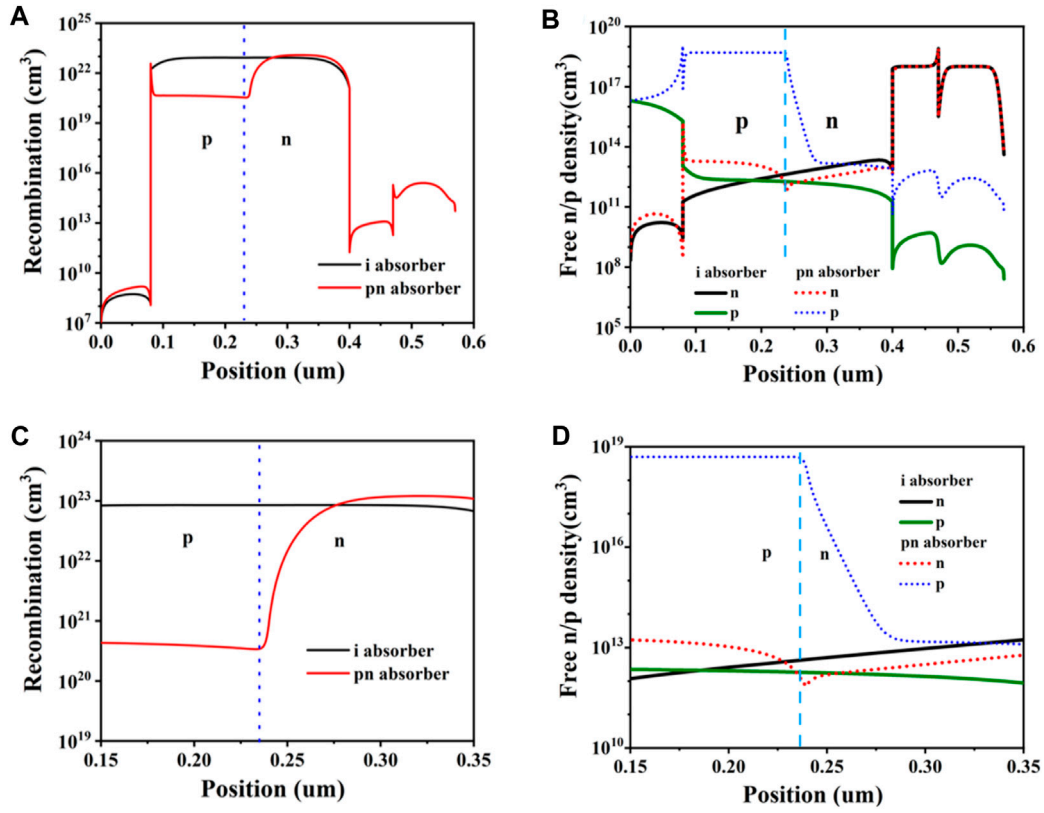


FIGURE. 3
**(A)** Recombination of two different structures **(B)** free electron and hole density plots of two different structures. **(C,D)** are enlarged figures of **(A,B)**, respectively.

Figure 4C is the band diagram of the device further calculated after the optimal doping concentration is obtained. It can be found that the P-N uniform junction leads to the intensification of the band bending, and the built-in electric field increases to a certain extent, which leads to the improvement of $V_{OC}$ (Baikie et al., 2013). As shown in Figure 4D, the calculated cell carrier density distribution shows that the electron density decreases and the hole density increases in the P-type perovskite region close to the hole transport layer, suggesting that the perovskite homologous junction promotes the directional carrier transport.

We can see from Figure 5A that the Planar P-N homologous junction solar cells have an average solar absorptivity of 88.58% in the range of 300 nm–800 nm, and the bands with absorptivities greater than 90% account for 59.57% of the whole band. In addition, Figure 5A depicts the distribution of electric field intensity at a wavelength of 655 nm within the PSCs. The plot reveals a noticeable periodic alteration in the perovskite absorbing layer in correspondence with guided mode resonance's standing wave features (Anand et al., 2022; Shangguan et al., 2022c; Zhang T. X. et al., 2022; Zhang Y. et al., 2023). A multitude of electric fields exist within the organic layer. When the intensity difference between interference fringes is significant, electric field interference distribution arises. The diagram illustrates that there is a greater intensity of electric field at the reflective layer and interface, promoting heightened light absorption. Then, the energy absorption and loss of planar P-N homojunction solar cells were calculated under AM1.5 conditions using a polarised incident plane wave (300 nm–800 nm) as the light source for the standard AM 1.5G solar spectrum (Di Giacomo et al., 2020; Jiang et al., 2021; Zheng et al., 2022; Li et al., 2023c; Wu et al., 2023), as depicted in Figure 5B. The results indicate that PSCs exhibit superior absorption performance for visible and near-infrared light.

## 4 Conclusion

The main focus of this study is to optimise the design of P-I-N PSCs and to analyse and evaluate a novel P-N homojunction PSCs.P-N homojunction refers to the doping of the same semiconducting material with different types of impurities, resulting in the formation of P-type and N-type regions as well as a built-in electric field. Through comparative experiments and theoretical simulations, this study found that the photovoltaic conversion efficiency of the P-N homojunction PSCs was increased by about 3% compared to the conventional P-I-N PSCs under the same conditions. This is mainly attributed to the fact that the P-N homojunction creates a larger energy band bending in the perovskite layer, which increases the $V_{OC}$. At the same time, the P-N homojunction also facilitates the reduction of interfacial complexation and the improvement of carrier transport properties. Furthermore, the optical properties of the cells were

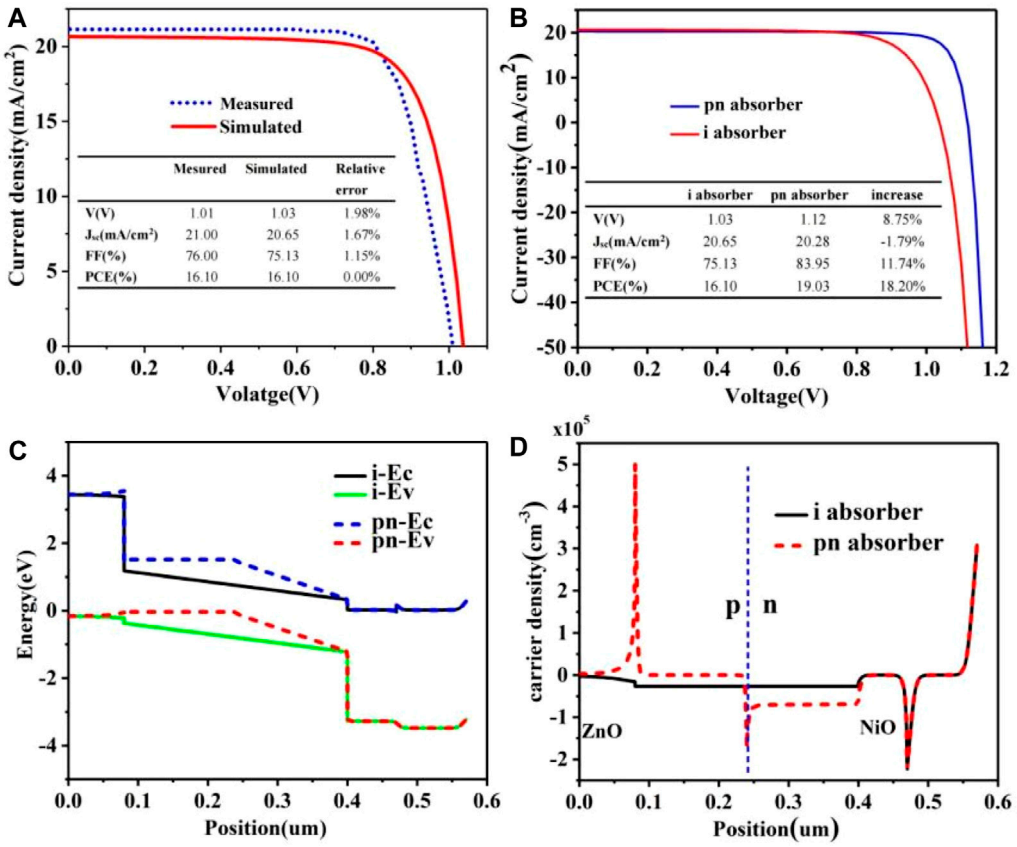


FIGURE. 4
**(A)** Comparison of PCE results between simulation and experiment; P-I-N structure and PN homologous junction structure, **(B)** Comparison of PCE; **(C)** Energy level diagram; **(D)** carrier density.

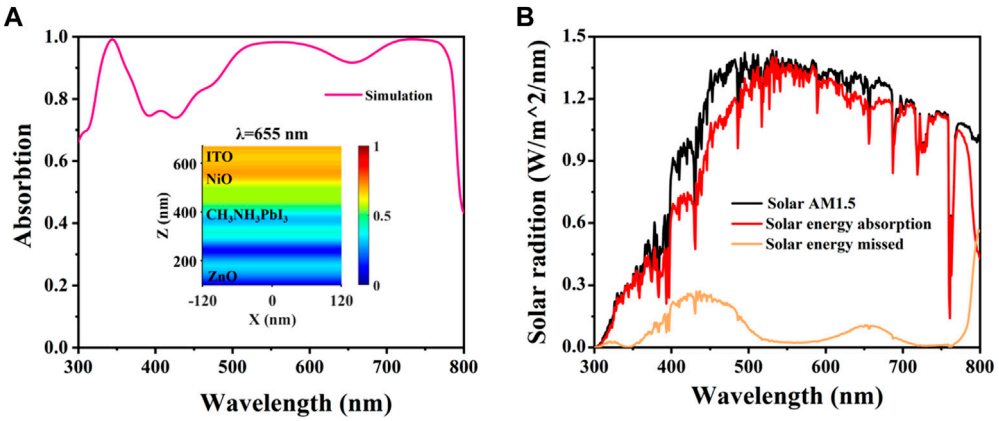


FIGURE. 5
**(A)** Absorption spectra of planar P-N homojunction solar cells and E-field intensity profiles at 655 nm **(B)** Solar energy absorption and loss spectra of optimized structures.

analyzed by analyzing the absorption spectrum and E-field intensity profiles. This study provides an effective performance optimisation method for conventional planar-structured PSCs, and offers new ideas for further exploration of the physical properties of perovskite materials and device design.

## Data availability statement

The original contributions presented in the study are included in the article/supplementary material, further inquiries can be directed to the corresponding authors.

## Author contributions

WL: Conceptualization, Data curation, Formal Analysis, Funding acquisition, Investigation, Methodology, Project administration, Resources, Software, Supervision, Validation, Visualization, Writing–original draft, Writing–review and editing. ZZ: Conceptualization, Data curation, Formal Analysis, Funding acquisition, Investigation, Methodology, Project administration, Resources, Software, Supervision, Validation, Visualization, Writing–original draft, Writing–review and editing. JZ: Conceptualization, Data curation, Formal Analysis, Funding acquisition, Investigation, Methodology, Project administration, Resources, Software, Supervision, Validation, Visualization, Writing–original draft, Writing–review and editing.

## Funding

The author(s) declare financial support was received for the research, authorship, and/or publication of this article. The authors are grateful to the support by the Scientific Research Fund of Zhejiang Provincial Education Department (Y202146019).

## Conflict of interest

The authors declare that the research was conducted in the absence of any commercial or financial relationships that could be construed as a potential conflict of interest.

## Publisher's note

All claims expressed in this article are solely those of the authors and do not necessarily represent those of their affiliated organizations, or those of the publisher, the editors and the reviewers. Any product that may be evaluated in this article, or claim that may be made by its manufacturer, is not guaranteed or endorsed by the publisher.

## References

Akihiro, K., Kenjiro, T., Yasuo, S., and Tsutomu, M. (2009). Organometal halide perovskites as visible-light sensitizers for photovoltaic cells. *J. Am. Chem. Soc.* 131 (17), 6050–6051. doi:10.1021/ja809598r

An, Y. D., Shang, A. X., Cao, G. Y., Wu, S. L., Ma, D., and Li, X. F. (2018). Perovskite solar cells: optoelectronic simulation and optimization. *Sol. RRL* 2, 1800126. doi:10.1002/solr.201800126

Anand, V., Han, M. L., Maksimovic, J., Ng, S. H., Katkus, T., Klein, A. R., et al. (2022). Single-shot mid-infrared incoherent holography using Lucy-Richardson-Rosen algorithm. *Opto-Electron Sci.* 1, 210006. doi:10.29026/oes.2022.210006

Azri, F., Meftah, A., Sengouga, N., and Meftah, A. (2019). Electron and hole transport layers optimization by numerical simulation of a perovskite solar cell. *Sol. energy* 181, 372–378. doi:10.1016/j.solener.2019.02.017

Baikie, T., Fang, Y., Kadro, J. M., Schreyer, M., Wei, F., Mhaisalkar, S. G., et al. (2013). Synthesis and crystal chemistry of the hybrid perovskite (CH3NH3)PbI3 for solid-state sensitised solar cell applications. *J. Mater. Chem. A* 1, 5628–5641. doi:10.1039/c3ta10518k

Chang, W. H., Tian, H. M., Fang, G. C., Guo, D., Wang, Z., and Zhao, K. Y. (2019). Simulation of innovative high efficiency perovskite solar cell with Bi-HTL: NiO and Si thin films. *Sol. Energy* 186, 323–327. doi:10.1016/j.solener.2019.05.017

Chatterji, N., and Pradeep, R. N. (2019). Electron versus hole extraction: self doping induced performance bottleneck in perovskite solar cells. *IEEE Electron Device Lett.* 40, 1784–1787. doi:10.1109/led.2019.2944474

Cui, P., Wei, D., Ji, J., Huang, H., Jia, E. D., Dou, S. Y., et al. (2019). Planar p–n homojunction perovskite solar cells with efficiency exceeding 21.3%. *Nat. Energy* 4, 150–159. doi:10.1038/s41560-018-0324-8

Di Giacomo, F., Castriotta, L. A., Kosasih, F. U., Di Girolamo, D., Ducati, C., and Di Carlo, A. (2020). Upscaling inverted perovskite solar cells: optimization of laser scribing for highly efficient mini-modules. *Micromachines* 11, 1127. doi:10.3390/mi11121127

Fu, W. F., Wang, Z. Y., Yi, Z., Song, Q. J., Bian, L., Cheng, S. B., et al. (2024). Optical design of ultra-thin GaAs solar cells based on trapezoidal pyramid structure. *Phys. B Condens. Matter* 677, 415708. doi:10.1016/j.physb.2024.415708

Guo, Y. M., Zhong, L. B., Min, L., Wang, J. Y., Wu, Y., Chen, K. L., et al. (2022). Adaptive optics based on machine learning: a review. *Opto-Electron. Adv.* 5, 200082. doi:10.29026/oea.2022.200082

Haider, S. Z., Anwar, H., and Wang, M. (2018). A comprehensive device modelling of perovskite solar cell with inorganic copper iodide as hole transport material. *Semicond. Sci. Technol.* 33, 035001. doi:10.1088/1361-6641/aaa596

He, L., Yi, Y. T., Zhang, J. G., Xu, X. B., Tang, B., Li, G. F., et al. (2024). A four-narrowband terahertz tunable absorber with perfect absorption and high sensitivity. *Mater. Res. Bull.* 170, 112572. doi:10.1016/j.materresbull.2023.112572

He, P. H., Niu, L. Y., Fan, Y., Zhang, H. C., Zhang, L. P., Yao, D., et al. (2022). Active odd-mode-metachannel for single-conductor systems. *Opto-Electron Adv.* 5, 210119. doi:10.29026/oea.2022.210119

He, Q. M., Gu, H. Y., Zhang, D. Q., Fang, G. C., and Tian, H. M. (2021). Theoretical analysis of effects of doping MAPbI into p-n homojunction on several types of perovskite solar cells. *Opt. Mater.* 121, 111491. doi:10.1016/j.optmat.2021.111491

Huang, L. K., Sun, X. X., Li, C., Xu, R., Xu, J., Du, Y. Y., et al. (2016). Electron transport layer-free planar perovskite solar cells: further performance enhancement perspective from device simulation. *Sol. Energy Mater. Sol. Cells* 157, 1038–1047. doi:10.1016/j.solmat.2016.08.025

Jiang, L. Y., Yi, Y. T., Yi, Z., Yang, H., Li, Z. Y., Su, J., et al. (2021). A four-band perfect absorber based on high quality factor and high figure of merit of monolayer molybdenum disulfide. *Acta Phys. Sin.* 70, 128101. doi:10.7498/aps.70.20202163

Kim, H.-S., Lee, C.-R., Im, J. H., Lee, K. B., Moehl, T., Marchioro, A., et al. (2012). Lead iodide perovskite sensitized all-solid-state submicron thin film mesoscopic solar cell with efficiency exceeding 9%. *Sci. Rep.* 2, 591. doi:10.1038/srep00591

Li, W., Ma, J., Zhang, H., Cheng, S., Yang, W., Yi, Z., et al. (2023b). Tunable broadband absorber based on a layered resonant structure with a Dirac semimetal. *Phys. Chem. Chem. Phys.* 25, 8489–8496. doi:10.1039/D2CP05562G

Li, W., Yi, Y., Yang, H., Cheng, S., Yang, W. X., Zhang, H., et al. (2023c). Active tunable terahertz bandwidth absorber based on single layer graphene. *Commun. Theor. Phys.* 75, 045503. doi:10.1088/1572-9494/acbe2d

Li, W. X., Liu, M. S., Cheng, S. B., Zhang, H. F., Yang, W. X., Yi, Z., et al. (2024a). Polarization independent tunable bandwidth absorber based on single-layer graphene. *Diam. Relat. Mater.* 142, 110793. doi:10.1016/j.diamond.2024.110793

Li, W. X., Xu, F., Cheng, S. B., Yang, W. X., Liu, B., Liu, M. S., et al. (2024b). Six-band rotationally symmetric tunable absorption film based on AlCuFe quasicrystals. *Opt. Laser Technol.* 169, 110186. doi:10.1016/j.optlastec.2023.110186

Li, W. X., Zhao, W. C., Cheng, S. B., Yang, W. X., Yi, Z., Li, G. F., et al. (2023a). Terahertz selective active electromagnetic absorption film based on single-layer graphene. *Surf. Interfaces* 40, 103042. doi:10.1016/j.surfin.2023.103042

Liang, S., Xu, F., Yang, H., Cheng, S., Yang, W., Yi, Z., et al. (2023a). Ultra long infrared metamaterial absorber with high absorption and broad band based on nano cross surrounding. *Opt. Laser Technol.* 158, 108789. doi:10.1016/j.optlastec.2022.108789

Liang, S. R., Xu, F., Li, W. X., Yang, W. X., Cheng, S. B., Yang, H., et al. (2023b). Tunable smart mid infrared thermal control emitter based on phase change material VO2 thin film. *Appl. Therm. Eng.* 232, 121074. doi:10.1016/j.applthermaleng.2023.121074

Lin, L. Y., Jiang, L. Q., Li, P., Fan, B. D., and Qiu, Y. (2019). A modeled perovskite solar cell structure with a Cu2O hole-transporting layer enabling over 20% efficiency by low-cost low-temperature processing. *J. Phys. Chem. Solids* 124, 205–211. doi:10.1016/j.jpcs.2018.09.024

Liu, T., Liu, Y., Ling, L., Sheng, Z., Yi, Z., Zhou, Z., et al. (2024). Multifunctional terahertz device with active switching between bimodal perfect absorption and plasmon-induced transparency. *Mater. Res. Bull.* 171, 112635. doi:10.1016/j.materresbull.2023.112635

Lu, W. Q., Wu, P. H., Bian, L., Yan, J. Q., Yi, Z., Liu, M. S., et al. (2024). Perfect adjustable absorber based on Dirac semi-metal high sensitivity four-band high

frequency detection. *Opt. Laser Technol.* 174, 110650. doi:10.1016/j.optlastec.2024.110650

Lu, W. Q., Yi, Z., Zhang, J. G., Xu, X. B., Tang, B., Li, G. F., et al. (2023). A tunable broadband absorber in the terahertz band based on the proportional structure of a single layer of graphene. *Diam. Relat. Mater.* 140, 110481. doi:10.1016/j.diamond.2023.110481

Ma, J., Tian, Y., Cheng, J., Cheng, S., Tang, B., Chen, J., et al. (2023a). Active broadband absorber based on phase-change materials optimized via evolutionary algorithm. *Coatings* 13, 1604. doi:10.3390/coatings13091604

Ma, J., Wu, P. H., Li, W. X., Liang, S. R., Shangguan, Q. Y., Cheng, S. B., et al. (2023b). A five-peaks graphene absorber with multiple adjustable and high sensitivity in the far infrared band. *Diam. Relat. Mater.* 136, 109960. doi:10.1016/j.diamond.2023.109960

Maksimovic, J., Hu, J. W., Ng, S. H., Katkus, T., Seniutinas, G., Pinedo Rivera, T., et al. (2022). Beyond Lambertian light trapping for large-area silicon solar cells: fabrication methods. *Opto-Electron Adv.* 5, 210086. doi:10.29026/oea.2022.210086

Maram, D. K., Haghighi, M., Shekoofa, O., Habibiyan, H., and Ghafoorifard, H. (2021). A modeling study on utilizing ultra-thin inorganic HTLs in inverted p–n homojunction perovskite solar cells. *Sol. Energy* 213, 1–12. doi:10.1016/j.solener.2020.11.009

Mohamad, I. S., Doroody, C., Alkharasani, W. M., Norizan, M. N., Chelvanathan, P., Shahahmadi, S. A., et al. (2023). Elucidating the effects of interconnecting layer thickness and bandgap variations on the performance of monolithic perovskite/silicon tandem solar cell by wxAMPS. *Materials* 16, 4106. doi:10.3390/ma16114106

Park, J., Kim, J., Yun, H. S., Paik, M. J., Noh, E., Mun, H. J., et al. (2023). Controlled growth of perovskite layers with volatile alkylammonium chlorides. *Nature* 616, 724–730. doi:10.1038/s41586-023-05825-y

Peng, H., Su, Z., Zheng, Z., Lan, H., Luo, J., Fan, P., et al. (2019). High-Quality perovskite CH3NH3PbI3 thin films for solar cells prepared by single-source thermal evaporation combined with solvent treatment. *Materials* 12, 1237. doi:10.3390/ma12081237

Sengar, B. S., Garg, V., Kumar, A., and Dwivedi, P. (2021). Numerical simulation: design of high-efficiency planar p-n homojunction perovskite solar cells. *IEEE Trans. Electron Devices* 68 (5), 2360–2364. doi:10.1109/TED.2021.3066454

Seyed-Talebi, S. M., Mahmoudi, M., and Lee, C.-H. (2023). A comprehensive study of CsSnI3-based perovskite solar cells with different hole transporting layers and back contacts. *Micromachines* 14, 1562. doi:10.3390/mi14081562

Shangguan, Q., Chen, H., Yang, H., Liang, S., Zhang, Y., Cheng, S., et al. (2022a). A "belfry-typed" narrow-band tunable perfect absorber based on graphene and the application potential research. *Diam. Relat. Mater.* 125, 108973. doi:10.1016/j.diamond.2022.108973

Shangguan, Q., Chen, Z., Yang, H., Cheng, S., Yang, W., Yi, Z., et al. (2022b). Design of ultra-narrow band graphene refractive index sensor. *Sensors* 22, 6483. doi:10.3390/s22176483

Shangguan, Q., Zhao, Y., Song, Z., Wang, J., Yang, H., Chen, J., et al. (2022c). High sensitivity active adjustable graphene absorber for refractive index sensing applications. *Diam. Relat. Mater.* 128, 109273. doi:10.1016/j.diamond.2022.109273

Shen, T. Y., Qin, J. J., Bai, Y. J., Zhang, J., Shi, L., Hou, X., et al. (2022). Giant magneto field effect in up-conversion amplified spontaneous emission via spatially extended states in organic-inorganic hybrid perovskites. *Opto-Electron Adv.* 5, 200051. doi:10.29026/oea.2022.200051

Vallisree, S., Thangavel, R., and Lenka, T. R. (2018). Theoretical investigations on enhancement of photovoltaic efficiency of nanostructured CZTS/ZnS/ZnO based solar cell device. *J. Mater Sci. Mater Electron* 29, 7262–7272. doi:10.1007/s10854-018-8715-y

Verschraegen, J., and Marc, B. (2007). Numerical modeling of intra-band tunneling for heterojunction solar cells in SCAPS. *Thin Solid Films* 515, 6276–6279. doi:10.1016/j.tsf.2006.12.049

Wang, D. Y., Yi, Z., Ma, G. L., Dai, B., Yang, J. B., Zhang, J. F., et al. (2022b). Two-channel photonic crystal fiber based on surface plasmon resonance for magnetic field and temperature dual-parameter sensing. *Phys. Chem. Chem. Phys.* 24, 21233–21241. doi:10.1039/D2CP02778J

Wang, D. Y., Zhu, W. L., Yi, Z., Ma, G. L., Gao, X., Dai, B., et al. (2022a). Highly sensitive sensing of a magnetic field and temperature based on two open ring channels SPR-PCF. *Opt. Express* 30, 39055. doi:10.1364/OE.470386

Wu, F. Y., Liu, Y. H., Ling, L., Sheng, Z. X., Yi, Z., Song, Q. J., et al. (2023). Spectrally selective ultra-broadband solar absorber based on pyramidal structure. *Adv. Photonics Res.* 2023, 2300305. doi:10.1002/adpr.202300305

Xiao, T. X., Tu, S., Liang, S. Z., Guo, R. J., Tian, T., and Müller-Buschbaum, P. (2023). Solar cell-based hybrid energy harvesters towards sustainability. *Opto-Electron Sci.* 2, 230011. doi:10.29026/oes.2023.230011

You, J. B., Meng, L., Song, T. B., Guo, T. F., Yang, Y., Chang, W. H., et al. (2016). Improved air stability of perovskite solar cells via solution-processed metal oxide transport layers. *Nat. Nanotech* 11, 75–81. doi:10.1038/nnano.2015.230

Zhang, C., Yi, Y., Yang, H., Yi, Z., Chen, X., Zhou, Z., et al. (2022a). Wide spectrum solar energy absorption based on germanium plated ZnO nanorod arrays: energy band regulation, Finite element simulation, Super hydrophilicity, Photothermal conversion. *Appl. Mater. Today* 28, 101531. doi:10.1016/j.apmt.2022.101531

Zhang, H., Feng, L., Wang, F. Y., Liu, M. Z., Zhang, Y. Y., Zhu, J., et al. (2023a). Janus aramid nanofiber aerogel incorporating plasmonic nanoparticles for high-efficiency interfacial solar steam generation. *Opto-Electron Adv.* 6, 220061. doi:10.29026/oea.2023.220061

Zhang, T. X., Tao, C., Ge, S. X., Pan, D. W., Li, B., Huang, W. X., et al. (2022c). Interfaces coupling deformation mechanisms of liquid-liquid-liquid three-phase flow in a confined microchannel. *Chem. Eng. J.* 434, 134769. doi:10.1016/j.cej.2022.134769

Zhang, Y., Yi, Y., Li, W., Liang, S., Ma, J., Cheng, S., et al. (2023b). High absorptivity and ultra-wideband solar absorber based on Ti-Al2O3 cross elliptical disk arrays. *Coatings* 13, 531. doi:10.3390/coatings13030531

Zhang, Y. T., and Xuan, Y. M. (2016). Comprehensive design of omnidirectional high-performance perovskite solar cells. *Sci. Rep.* 6, 29705. doi:10.1038/srep29705

Zhang, Y. X., Pu, M. B., Jin, J. J., Lu, X. J., Guo, Y. H., Cai, J., et al. (2022b). Crosstalk-free achromatic full Stokes imaging polarimetry metasurface enabled by polarization-dependent phase optimization. *Opto-Electron Adv.* 5, 220058. doi:10.29026/oea.2022.220058

Zheng, R. Y., Liu, Y. H., Ling, L., Sheng, Z. X., Yi, Z., Song, Q. J., et al. (2024b). Ultra wideband tunable terahertz metamaterial absorber based on single-layer graphene strip. *Diam. Relat. Mater.* 141, 110713. doi:10.1016/j.diamond.2023.110713

Zheng, Y., Wang, Z. Y., Yi, Z., Cheng, S. B., Ma, C., Tang, B., et al. (2024a). A wide-band solar absorber based on tungsten nano-strip resonator group and graphene for near-ultraviolet to near-infrared region. *Diam. Relat. Mater.* 142, 110843. doi:10.1016/j.diamond.2024.110843

Zheng, Z., Luo, Y., Yang, H., Yi, Z., Zhang, J., Song, Q., et al. (2022). Thermal tuning of terahertz metamaterial absorber properties based on $VO_2$. *Phys. Chem. Chem. Phys.* 24, 8846–8853. doi:10.1039/D2CP01070D

Zhu, W. L., Yi, Y. T., Yi, Z., Bian, L., Yang, H., Zhang, J. G., et al. (2023b). High confidence plasmonic sensor based on photonic crystal fibers with a U-shaped detection channel. *Phys. Chem. Chem. Phys.* 25, 8583–8591. doi:10.1039/D2CP04605A

Zhu, Y. Y., Cheng, J. Y., Yi, Z., Tang, B., Chen, J., Zhang, J. G., et al. (2023a). Spectrally selective solar absorber and thermal infrared suppression based on hollow cylindrical microstructures. *Opt. Commun.* 549, 129910. doi:10.1016/j.optcom.2023.129910